Materials Research. 2022; 25:e20220336
DOI: https://doi.org/10.1590/1980-5373-MR-2022-0336

Artificial Neural Networks for Producing a Low-Cost Austempered Ductile Iron

Diogo Hofmam*[a] , ***Fabiano Dornelles Ramos*[b,c]**, ***Guilherme Vieira Braga Lemos*[c,d]**,

***Cleber Rodrigo de Lima Lessa*[a,b]**

[a]*Instituto Federal do Rio Grande do Sul (IFRS), Programa de Pós-Graduação em Tecnologia e Engenharia de Materiais, Caxias do Sul, RS, Brasil.*
[b]*Instituto Federal do Rio Grande do Sul (IFRS), Caxias do Sul, RS, Brasil.*
[c]*Universidade Federal do Rio Grande do Sul (UFRGS), Programa de Pós-Graduação em Engenharia de Minas, Metalúrgica e de Materiais (PPGE3M), Porto Alegre, RS, Brasil.*
[d]*Universidade Federal de Santa Maria (UFSM), Cachoeira do Sul, RS, Brasil.*

Received: July 26, 2022; Revised: October 21, 2022; Accepted: October 25, 2022

Two artificial neural networks (ANNs) were developed for producing an austempered ductile iron (ADI) with low-cost chemical composition and mechanical properties as per ASTMA897/897M-16-grade-1050/750/07 standard. Thus, the first ANN predicted the chemical composition range within the lowest cost and required mechanical properties. Next, in the second ANN, the resulting values from the first ANN were refined considering the target chemical composition suggested in the standard. Moreover, mechanical properties and microstructural analyses were undertaken in the ADI produced to support the ANNs' findings. Hence, ANNs can be used to make a standard-compliant ADI and achieve cost savings.

Keywords: *Austempered ductile iron, Artificial neural network, Mechanical properties, Cost-savings.*

1. Introduction

The mechanical properties of cast irons make them interesting for applications such as gearboxes, connecting rods, and wheel hubs, amongst others[1]. Overall, the microstructure of ductile cast iron (DCI) is composed by ferrite and pearlite with nodular graphite[2]. Besides, low-cost production with improved yield strength (YS) and ultimate tensile strength (UTS) through the austempering process can be reached[3]. The mechanical properties are classified in ASTM A897/A897M-16[4] to ensure reliability for producing ADI. Thus, austempering process consists of austenitising at 815-925°C to generate an austenite microstructure (γ), followed by quenching at 260-400°C for the process to occur[5,6]. The resulting microstructure is acicular ferrite, which might be called ausferrite in a carbon saturated austenite matrix[7-10].

Artificial neural networks (ANN) can be used in varied engineering fields due to their excellent self-learning function. ANNs are a potential tool for forecasting various consequences of the manufacturing process[11,12]. Cao and Guo[11] showed that the cutting force for machining an ADI was successfully estimated using ANN, with an error of around 4%. Hammood and Lieth[13] presented ANN for the effect of retained austenite on fatigue life, and the mechanical properties were predicted with high accuracy. Guo[14] analysed the hardness through ANN and varied austempering parameters, and thus the predicted values approached the measured data. Ławrynowicz and Dymski[15] compared the mechanical properties of ADI through an algorithm showing that ANN is suitable for analysing the ultimate tensile strength (UTS), yield strength (YS), and elongation.

The current work aims at producing an ADI with low-cost chemical composition and required mechanical properties by applying ANNs. Thus, these mechanical properties are as per ASTM A897/897M - 16 Grade 2 1050/750/07 standard.

2. Materials and Methods

2.1. Database

The current investigation was based on reports and technical sheets related to ADI production[16-37]. The database was organised with a variation in the chemical compositions (low to high levels of alloying elements) seventy-five chemical compositions with thirteen alloying elements (C, Si, Mn, Mo, Ni, Mg, S, Cu, Cr, Ti, Al, V, Nb) and their mechanical properties (UTS) [MPa], YS [MPa], elongation [%], and hardness Brinell [HB]). All these are required following ASTM A897/897M-16. So, this database was used for calculating the furnace charge and estimating the cost variation [$/ton].

2.2. The furnace charge, cost variation, and dataset

The charge calculation estimated a minimum of a ton of cast iron for each alloy[38]. The primary raw materials were pig iron, steel scrap, and ferroalloys. To that, the data from the international market[39] and the Brazilian Foundry Association[40] were used, and quantities for producing cast iron in the charge, and the gross cost was estimated[40,41]. Therefore, the

*e-mail: diogo.hofmam@outlook.com

alloy cost was obtained by its variation between different charges. The minimum cost was identified as "100%", up to a maximum of "472.71%". Thus, a dataset containing variables as costs in charge and chemical compositions with their mechanical properties (C, Si, Mn, Mo, Ni, Mg, S, Cu, Cr, Ti, Al, V, Nb, cost variation [$/ton], YS, UTS, %E, and HB), totalling 1350 pieces of information. Table 1 shows a significant price variation.

2.3. Artificial neural network models, inputs, and outputs

An ANN model involves computations and mathematics for simulating the human–brain processes. ANNs have a specific architecture format, and regression models between data collection and analysis, structure design, hidden layers, simulation, and weights/bias trade-off computed through learning and training methods. Using an error optimisation algorithm (Levenberg-Marquardt (LMT), the ANN could find optimum weight for each synapse (the connection between nodes of different layers) after a certain number of epochs. Once the ANN is successfully trained, input parameters can be fed into the model, and afterwards, the ANN can predict the output parameters. In the current investigation, the ANN models were made using MATLAB software. The architecture of the LMT algorithm had multiple layers of the backpropagation type, which led to a superior performance in heat treatment[42]. The mean square error (MSE) was calculated using:

$$MSE = \frac{1}{N}\sum_{i=1}^{N}(f_i - y_i)^2$$

where N is the number of data points, f_i is the value returned by the model, and y_i is the actual value for data point "i". The MSE was obtained from the ANN training session.

The calculation of the partial derivatives of error concerning the parameters of the ANN is essential[43]. Thus, the accuracy (R^2) was used as a good indicator; when R^2 was close to 1, it meant maximum accuracy[44].

The first ANN was designed and trained using the LMT algorithm from the dataset information. Therefore, the LMT algorithm correlated the data by cross-referencing them using 70% for training, 15% for validation, and 15% for testing with these percentages based on[45,46]. The first ANN was constructed using minimum values simulated according to the standard (UTS 1050 MPa, YS 750 MPa, %E ~7, 302 HB, and $/ton < 100% (in Table 1); thus, the minimal requirements of these properties could lead to the lowest ADI cost. The minimum values were tested sixty-five times, which resulted in a certain range for each element. The first ANN is shown in Figure 1, and its architecture containing one hidden layer with seventeen nodes is next presented in Figure 2. Moreover, the second ANN is also shown in Figure 1, and its architecture comprising one hidden layer with seventeen nodes is further displayed in Figure 3.

In Figure 2, the architecture of the first ANN shows five input data values (UTS, YS, %E, HB, and $/ton). Therefore, this ANN contained one hidden layer with seventeen nodes and thirteen output element values (chemical composition).

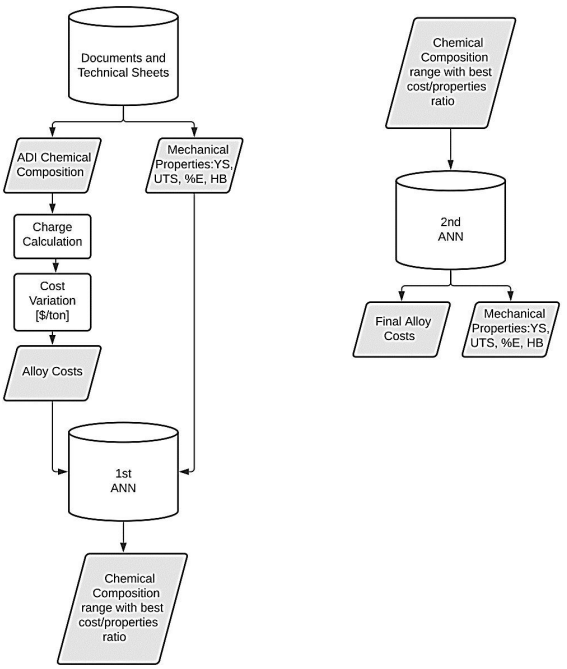

Figure 1. Flowchart showing the two ANNs of this work.

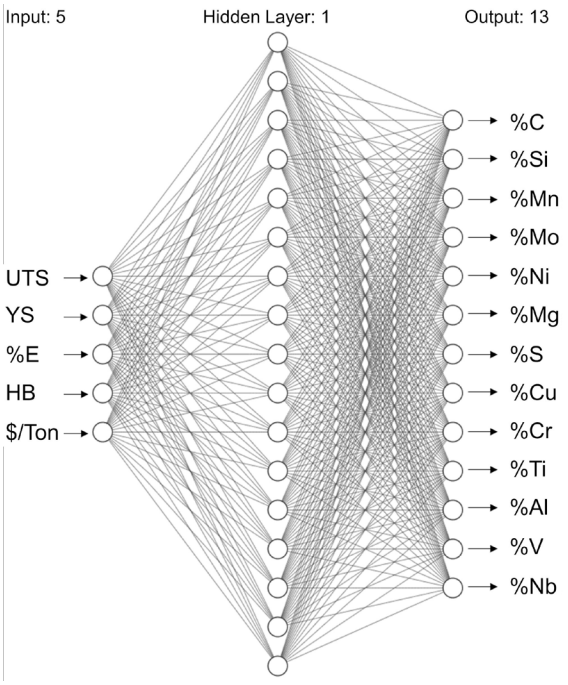

Figure 2. Architecture of the first ANN.

Table 1. Cost variation (%) between chemical compositions.

Sample	1	2	3	...	72	73	74	75
%	100.00%	102.76%	103.11%	...	257.79%	289.45%	359.41%	472.71%

Figure 3 shows the second ANN, where the input layer was the outcomes from the first ANN (chemical composition range tested), with one hidden layer, seventeen nodes, and five outputs (UTS, YS, %E, HB, and $/ton). The chemical composition range obtained in the first ANN (low and high quantities of alloying elements) was tested ten times at each level in the second ANN, thus equalling twenty trials. Thus, the second ANN was programmed to verify if the resulting chemical composition range of the first ANN implied a chemical composition that led to the required mechanical properties.

2.4. Casting and heat treatment

The molten metal with the resulting chemical composition was prepared in an induction electric furnace Inductotherm with a 1500 kg/hr capacity. Five Y-blocks of 25 mm thickness were pouring, and their dimensions are displayed in Figure 4.

After casting, the five Y-blocks were heat treated. In this context, based on the literature[2,16,18,24], the temperature for austenitisation was 850°C, and for austempering, it was 350°C. Considering these temperatures, the steps of the heat treatment were selected. Therefore, as shown in Figure 5, the alloy was austenitised for 30 minutes at 840°C (austenitising step) in a muffle furnace. After quenching, the austempering process was done for 30 minutes at 340°C in a quenching tank with a molten salt bath (sodium and potassium nitrate, $NaNO_3 + KNO_3$). Later, the samples were washed in hot water[47-49].

Samples with 58 mm length and 13 mm diameter were extracted for tensile tests, as per ASTM A897/A897M-16[4]. Furthermore, hardness measurements were performed in a Brinell Hardness tester with a 3000 kg load, as indicated in ASTM A897/897M - 2016. Complementarily, microhardness tests were carried out on a Mitutoyo HV 100 machine with a 1-kilogram load (HV1) due to the resulting microstructure. Thus, five measurements were performed in the ausferrite phase, and an average and standard deviation were calculated.

For microstructure investigation, samples were cut, prepared according to metallography, and etched using 3% Nital. The microstructure was analysed by optical microscopy (OM) in an OLYMPUS and scanning electron microscopy (SEM) in a SHIMADSU SSX-550[47]. In addition, the degree of nodularization was verified through comparison with images of[50]. Next, grain size and nodule count were measured using ImageJ software[51].

3. Results and Discussion

In Table 2, the resulting chemical composition range verified in the first ANN is presented. The suitability of the models proposed can be demonstrated through the R^2 scores achieved. Thus, Figure 6 shows that the R^2 scores of the first ANN were above 98%.

The chemical composition of ADI verified in the first ANN was evaluated by a spectrometer, and it is given in Table 3. In other words, the chemical composition predicted by the ANN was compared to that found in the ADI produced.

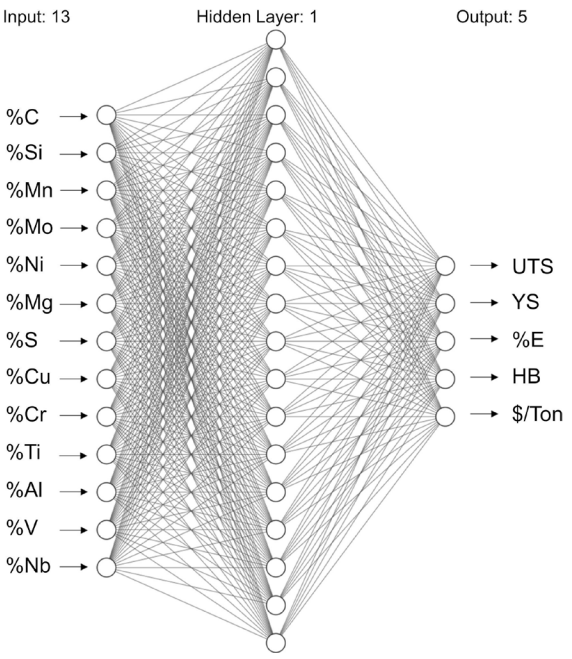

Figure 3. Architecture of the second ANN.

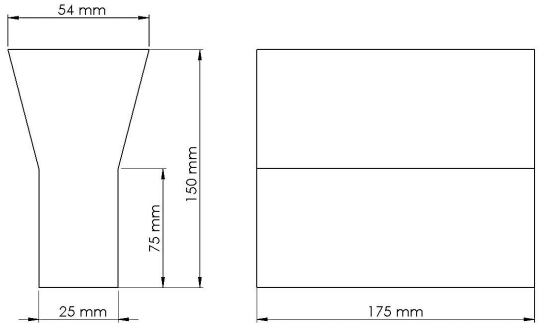

Figure 4. Y-block dimensions.

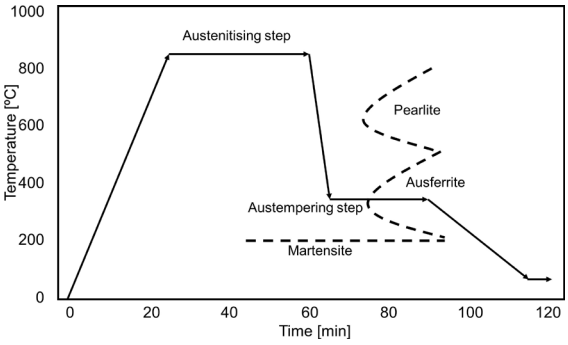

Figure 5. Heat treatment steps for ADI production.

Table 2. Chemical composition range in the first ANN.

	%C	%Si	%Mn	%Mo	%Ni	%Mg	%S	%Cu	%Cr	%Ti	%Al	%V	%Nb
Min.	3.60	2.40	0.50	0.00	0.01	0.05	0.01	0.05	0.05	0.00	0.02	0.00	0.00
Max.	3.70	2.50	0.60	0.00	0.02	0.06	0.01	0.05	0.06	0.00	0.10	0.00	0.00

Figure 7 presents the ausferrite phase, with characteristics such as needle-shaped acicular ferrite and stabilised austenite. Moreover, these results have similarities with the study of Mrzygłód B[10], where an ADI was austenitised at 920°C and austempered in salt baths at varying temperatures including a similar as used in this investigation. However, it should be noted that the present work attempted the production of ADI with a low amount of alloying elements, which thus led to a lower final cost. Figure 7a shows the graphite nodule, stabilized austenite, and acicular ferrite, as likewise seen by other authors[52,53]. Thus, in this way, our outcomes agree well with related studies on ADI[10,52,53]. Figure 7b presents SEM imaging analysis detailing the results shown in the OM. Finally, with graphite type I, the average nodule count was 362 nodules/mm^2. In addition, the degree of nodularization was 95%, and the average size of graphite was 35.69 µm. Therefore, it is noted that these findings follow ASTM A247 – 17[50].

In Figure 8, tensile testing results are shown by comparing the ADI produced, the standard, and three alloys found in literature[18,24,25], which works were selected as they reported an improvement in UTS due to the greater amount of ausferrite. However, Sellamuthu, P. and Jiwang Z[2,33]. employed a great quantity of alloying elements, which would lead to high costs. Therefore, the non-necessity of high number of alloying elements for achieving desired mechanical properties affects the cost production. The ADI produced shows one of the highest in UTS, besides being up to 81.23% cheaper compared to the selected alloys[18,24,25]. In addition, the indicated hardness range for ASTM A897/897M – 2016 grade 2 considering the microstructure formed is 302-375 HB: the current work achieved 354 HB, which is suitable. Putanda K. S[25]. obtained a hardness like the ADI as our study but with a high amount of alloying elements, thus demonstrating the importance of this work. Furthermore, microhardness measurements were done in the ausferrite phase, thus achieving an average of 382 HV (σ ±9.633).

In Figure 9, the average cost of the alloys used for the ANN development was 49.8% higher than the cost of the

Table 3. Manufactured chemical composition ADI alloy (wt%).

	%C	%Si	%Mn	%Mo	%Ni	%Mg	%S	%Cu	%Cr	%Ti	%Al	%V	%Nb
Sample	3.69	2.42	0.54	0.00	0.01	0.05	0.01	0.02	0.05	0.00	0.02	0.00	0.00

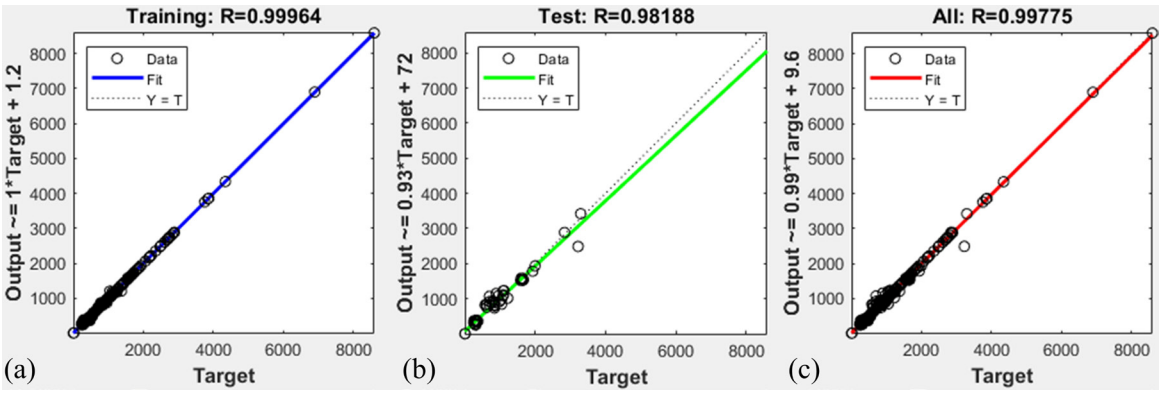

Figure 6. First ANN R2 scores (a) training 99.96%, (b) test 98.2% and (c) all 99.77%.

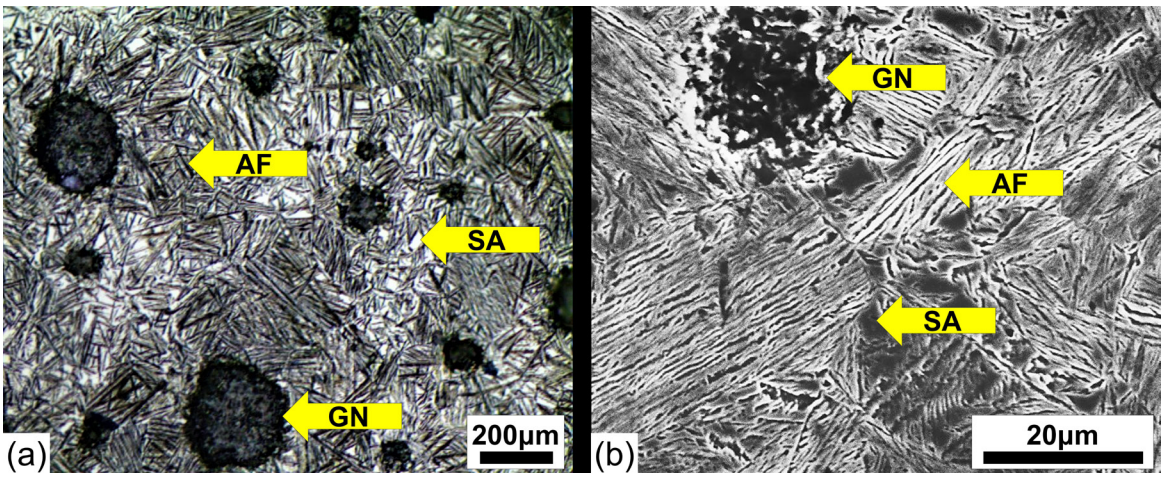

Figure 7. ADI microstructure (a) optical microscopy, where GN is Graphite Nodule, SA is Stabilised Austenite, and AF is Acicular Ferrite. (b) SEM imaging.

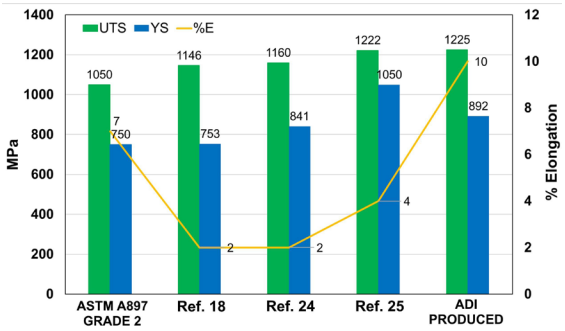

Figure 8. Comparison of mechanical properties of the ADI produced, three reports from the literature[18,24,25], and requirements of ASTM A897/897M – 16 Grade 2.

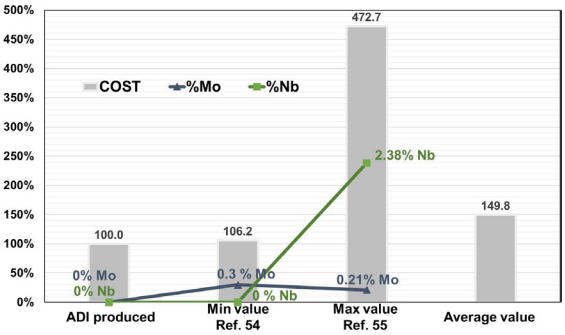

Figure 9. Cost comparison between alloys. Percentage (%) was defined as: ADI produced is 100%, and minimum and maximum values stand for the difference in relation to the ADI produced.

ADI produced. Moreover, these values are also shown as the amount of Mo and Nb plays an essential role in cost savings. Therefore, the ADI manufactured was 6.2% cheaper than the minimum value of the alloy[54]. In addition, the most expensive alloy (maximum value) costs 372.7%[55] more than the ADI produced. Thus, a low-cost ADI was manufactured, with requirements of microstructure and mechanical properties as per the standard[4]. Furthermore, both quantities of Mo and Nb in the ADI produced were basically zero, which agrees with its lowest cost.

4. Conclusions

i) A low-cost chemical composition was predicted through artificial neural networks (ANNs) for producing an austempered ductile cast iron (ADI). Next, chemical composition and mechanical properties were analysed in the manufactured ADI. Therefore, the ADI produced met the requirements of the ASTM A897/897M – 16 Grade 2 1050/750/07 standard.

ii) The architecture of the first and second ANNs using the Levenberg–Marquardt algorithm (LMT) was effective for predicting a low-cost chemical composition, mechanical properties, and final cost of ADI. Furthermore, the microstructure of the ADI manufactured was characterised by ausferrite with stabilised austenite.

iii) An ADI was produced with a considerable cost reduction compared to the costs of the alloys used in the database for developing the ANNs. Thus, the ADI manufactured was around 49% cheaper than the average cost of the alloys considered. However, a cost reduction during manufacturing cast parts might be complex and should be analysed in each specific context.

5. References

1. Korkmaz S. A methodology to predict fatigue life of cast iron: uniform material law for cast iron. J Iron Steel Res Int. 2011;18(8):42-5.
2. Sellamuthu P, Samuel DGH, Dinakaran D, Premkumar V, Li Z, Seetharaman S. S. Austempered ductile iron (ADI): influence of austempering temperature on microstructure, mechanical and wear properties and energy consumption. Metals. 2018;8(1):53.
3. Imasogie BI, Afonja AA, Ali JA. Properties of ductile cast iron nodularised with multiple calcium-magnesium based master alloy. Mater Sci Technol. 2000;16(2):194-201.
4. ASTM: American Society for Testing and Materials. ASTM A897/897M-2016: standard specification for austempered ductile iron castings. West Conshohocken: ASTM; 2016.
5. Cakir MC, Bayram A, Isik Y, Salar B. The effects of austempering temperature and time onto the machinability of austempered ductile iron. Mater Sci Eng A. 2005;407(1-2):147-53.
6. Panneerselvam S, Putatunda SK, Gundlach R, Boileau J. Influence of intercritical austempering on the microstructure and mechanical properties of austempered ductile cast iron (ADI). Mater Sci Eng A. 2017;694:72-80.
7. Savangouder RV, Patra JC, Bornand C. Prediction of hardness of austempered ductile iron using enhanced multilayer perceptron based on Chebyshev expansion. Commun Comput Inf Sci. 2019;1143:414-22.
8. Wang B, Barber G, Sun X, Shaw M, Seaton P. Characteristics of the transformation of retained austenite in austempered tempered ductile iron. J Mater Eng Perform. 2017;26(5):2095-101.
9. Silva ALVC, Mei PR. Aços e ligas especiais. São Paulo: Blucher; 2021.
10. Mrzygłód B, Kowalski A, Olejarczyk-Wozenska I, Giętka T, Głowacki M. Characteristics of ADI ductile cast iron with single addition of 1.56% Ni. Arch Metall Mater. 2017;62(4):2273-80.
11. Cao D, Guo XH. Prediction of cutting force of austempered ductile iron based on BP neural network. Adv Mat Res. 2013;774–776:1068-74.
12. Moutarde PF. Introduction to (shallow) neural networks. Paris: Centre For Robotics MINES ParisTech; 2021. 22 p.
13. Hammood AS, Lieth HM. A study the effect of retained austenite on fatigue life of austempering ductile iron by using artificial neural networks. Int J Curr Eng Technol. 2013;3(5):1946-51.
14. Guo X. Correlation between austempering parameters and hardness of austempered ductile iron based on artificial neural network. Comput. Model. New Technol. 2014;18(3):72-6.
15. Ławrynowicz Z, Dymski S. Neural network analysis of tensile properties of austempered ductile iron. Adv. Mater. Sci. 2008;8(1):94-104.
16. Kovacs BV. Development of austempered ductile iron (ADI) for automobile crankshafts. J Heat Treat Mater. 1987;5(1):55-60.
17. Petersen DR, Link RE, Putatunda SK, Singh I. Fracture toughness of unalloyed austempered ductile cast iron (ADI). J Test Eval. 1995;23(5):325-32.
18. Zimba J, Simbi DJ, Navara E. Austempered ductile iron: an alternative material for earth moving components. Cement Concr Compos. 2003;25(6):643-9.
19. Souza SAR. Influência do alumínio nas propriedades mecânicas do ADI [thesis]. Belo Horizonte: Universidade Federal de Minas Gerais; 2004.

20. Shelton P, Bonner A. The effect of copper additions to the mechanical properties of austempered ductile iron (ADI). J Mater Process Technol. 2006;173(3):269-74.
21. Putatunda S, Kesani S, Tackett R, Lawes G. Development of austenite free ADI (austempered ductile cast iron). Mater Sci Eng A. 2006;435-436:112-22.
22. Putatunda SK. Development of austempered ductile cast iron (ADI) with simultaneous high yield strength and fracture toughness by a novel two-step austempering process. Mater Sci Eng A. 2001;315:70-80.
23. Kim Y-J, Shin H, Park H, Lim JD. Investigation into mechanical properties of austempered ductile cast iron (ADI) in accordance with austempering temperature. Mater Lett. 2008;62(3):357-6.
24. Mattar AR Jr. Influência dos elementos de liga Cu-Ni-Mo nas propriedades mecânicas e na austemperabilidade do ADI [thesis]. São Paulo: Universidade de São Paulo; 2009.
25. Putatunda SK. Comparison of the mechanical properties of austempered ductile cast iron (ADI) processed by conventional and step-down austempering process. Mater Manuf Process. 2010;25(8):749-57.
26. Basso A, Caldera M, Chapetti M, Sikora J. Mechanical characterization of dual phase austempered ductile iron. ISIJ Int. 2010;50(2):302-6.
27. Sahoo S. A study on the effect of austempering temperature, time and copper addition on the tensile properties of austempered ductile iron [thesis]. Rourkela: National Institute of Technology; 2011.
28. Mattar AR, Heck SC, Neto AL, Fernandes F A P, Totten GE, Casteletti LC. Influence of alloying elements Cu, Ni and Mo on mechanical properties and austemperability of austempered ductile Iron. Int Heat Treat Surf Eng. 2011;5(2):78-82.
29. Guesser WL, Koda F, Martinez JAB, Silva CH. Austempered ductile iron for gears. Warrendale: SAE International; 2012. (SAE Technical Papers).
30. Padan DS. Microalloying in austempered ductile iron (ADI). Trans Amer Foundry Soc. 2012;120:277-88.
31. Kowalskia A, Kloska-Nawarecka S, Regulski K. ADI after austenitising from intercritical temperature. Arch. Foundry Eng. 2013;13(1):81-8.
32. Das A, Dhal J, Panda R, Mishra SC, Sen S. Effect of alloying elements and processing parameters on mechanical properties of austempered ductile iron. J. Mater Metal Eng. 2013;3:8-16.
33. Zhang J, Zhang N, Zhang M, Lu L, Zeng D, Song Q. Microstructure and mechanical properties of austempered ductile iron with different strength grades. Mater Lett. 2014;119:47-50.
34. Panneerselvam S, Martis CJ, Putatunda SK, Boileau JM. An investigation on the stability of austenite in austempered ductile cast iron (ADI). Mater Sci Eng A. 2015;626:237-46.
35. Basso A, Caldera M, Massone J. Development of high silicon dual phase austempered ductile iron. ISIJ Int. 2015;55(5):1106-13.
36. Méndez S, de la Torre U, González-Martínez R, Súarez R. Advanced properties of ausferritic ductile iron obtained in as-cast conditions. Inter Metalcast. 2017;11:116-22.
37. Olawale O, Ibitoye S, Oluwasegun K, Shittu M, Popoola P. Forced-air cooling quenching: a novel technique for austempered ductile iron production. Int. J. Met. 2016;11:1.
38. Seidu SO, Onigbajumo A. Development of charge calculation program for target steel in induction furnace. LEJPT. 2015;14(27):81-97.
39. Fastmarkets [Internet]. London; 2021 [cited 2021 Aug 10]. Available from: https://www.fastmarkets.com/commodities
40. ABIFA: Associação Brasileira de Fundição [Internet]. São Paulo; 2021 [cited 2021 Sept 2]. Available from: https://abifa.org.br/
41. Metal Bulletin [Internet]. London; 2021 [cited 2021 Oct 28]. Available from: https://www.metalbulletin.com/steel/steel-raw-materials/ferrous/hbi-pig-iron-and-dri.html
42. Agbeleye A, Esezobor D, Agunsoye J, Balogun SA, Sosimi AA. Prediction of the abrasive wear behaviour of heat-treated aluminium-clay composites using an artificial neural network. J Taibah Univ Sci. 2018;12(2):235.
43. Biernacki R, Kozłowski J, Myszka D, Perzyk M. Prediction of properties of austempered ductile iron assisted by artificial neural network. Inst Mater Proc. 2006;12(1):11-5.
44. Masood Chaudry U, Hamad K, Abuhmed T. Machine learning-aided design of aluminum alloys with high performance. Mater Today Commun. 2021;26:101897.
45. Khan I, Raja MAZ, Shoaib M, Kumam P, Alrabaiah H, Shah Z, et al. Design of neural network with Levenberg-Marquardt and Bayesian regularization backpropagation for solving pantograph delay differential equations. IEEE Access. 2020;8:137918-33.
46. Lv C, Xing Y, Zhang J, Na X, Li Y, Liu T, et al. Levenberg-Marquardt backpropagation training of multilayer neural networks for state estimation of a safety-critical cyber-physical system. IEEE Trans Industr Inform. 2018;14(8):3436-46.
47. Konca E, Tur K, Koç E. Effects of alloying elements (Mo, Ni, and Cu) on the austemperability of GGG-60 ductile cast iron. Metals. 2017;7(8):320.
48. Boccardo AD, Dardati PM, Celentano DJ, Godoy LA. Austempering heat treatment of ductile iron: computational simulation and experimental validation. Finite Elem Anal Des. 2017;134:82-91.
49. Boccardo AD, Dardati PM, Godoy LA, Celentano DJ. Sensitivity of austempering heat treatment of ductile irons to changes in process parameters. Metall Mater Trans, B, Process Metall Mater Proc Sci. 2018;49(3):1522-36.
50. ASTM: American Society for Testing and Materials. ASTM A247-2019: standard test method for evaluating the microstructure of graphite in iron castings. West Conshohocken: ASTM; 2019.
51. ASTM: American Society for Testing and Materials. ASTM E112-2010: standard test methods for determining average grain Size. West Conshohocken: ASTM; 2010.
52. Olawale JO, Ibitoye SA. Influence of casting section thickness on fatigue strength of austempered ductile iron. J Mater Eng Perform. 2017;26(10):4997-5008.
53. Kutsov A, Taran Y, Uzlov K, Krimmel A, Evsyukov M. Formation of bainite in ductile iron. Mater Sci Eng A. 1999;273-275:480-4.
54. Sellamuthu P, Samuel DGH, Dinakaran D, Premkumar V, Li Z, Seetharaman S. Austempered ductile iron (ADI): influence of austempering temperature on microstructure, mechanical and wear properties and energy consumption. Metals. 2018;8(1):53.
55. Pimentel ASO, Guesser WL, Silva WJRC, Portella PD, Woydt M, Burbank J. Abrasive wear behavior of austempered ductile iron with niobium additions. Wear. 2019;440-441:203065.